Thermal resistance matrix representation of thermal effects and thermal design in multi-finger power heterojunction bipolar transistors*

Jin Dong-Yue(金冬月)†, Zhang Wan-Rong(张万荣), Chen Liang(陈 亮), Fu Qiang(付 强), Xiao Ying(肖 盈), Wang Ren-Qing(王任卿), and Zhao Xin(赵 昕)

College of Electronic Information and Control Engineering, Beijing University of Technology, Beijing 100124, *China*

(Received 19 November 2010; revised manuscript received 15 December 2010)

The thermal resistance matrix including self-heating thermal resistance and thermal coupling resistance is presented to describe the thermal effects of multi-finger power heterojunction bipolar transistors. The dependence of thermal resistance matrix on finger spacing is also investigated. It is shown that both self-heating thermal resistance and thermal coupling resistance are lowered by increasing the finger spacing, in which the downward dissipated heat path is widened and the heat flow from adjacent fingers is effectively suppressed. The decrease of self-heating thermal resistance and thermal coupling resistance is helpful for improving the thermal stability of power devices. Furthermore, with the aid of the thermal resistance matrix, a 10-finger power heterojunction bipolar transistor (HBT) with non-uniform finger spacing is designed for high thermal stability. The optimized structure can effectively lower the peak temperature while maintaining a uniformity of the temperature profile at various biases and thus the device effectively may operate at a higher power level.

Keywords: heterojunction bipolar transistor, power, thermal stability, thermal resistance matrix

PACS: 44.10.+i, 73.40.Lq, 91.60.Ki **DOI:** 10.1088/1674-1056/20/6/064401

1. Introduction

For power heterojunction bipolar transistors (HBTs), a multiple emitter finger structure shown in Fig. 1 has been widely used to spread the current and the dissipated heat in which several emitter fingers are arranged in the direction parallel to each other and finger spacings are all identical.[1,2] However, the self-heating effect caused by the power dissipation and the thermal-coupling effect among emitter fingers result in a higher temperature in the central fingers of the device. Because of the positive temperature coefficient of collector current, the central fingers will conduct more currents and generate more heat, which will give rise to the thermal instability of power HBTs,[3,4] and leads their power-handling capability to be considerably below electrical limitation.[5−7]

In order to represent the self-heating and thermal coupling effects, thermal resistance matrix ($[R_{ij}]$) including self-heating thermal resistance (R_{ii}) and thermal coupling resistance ($R_{ij(i\neq j)}$) is proposed in the paper. The dependence of $[R_{ij}]$ on finger spacing is also studied. Furthermore, with the aid of $[R_{ij}]$, the multi-finger power HBT with non-uniform finger spacing is designed to lower the peak temperature, improve the non-uniformity of the temperature profile and hence enhance the thermal stability of power HBTs.

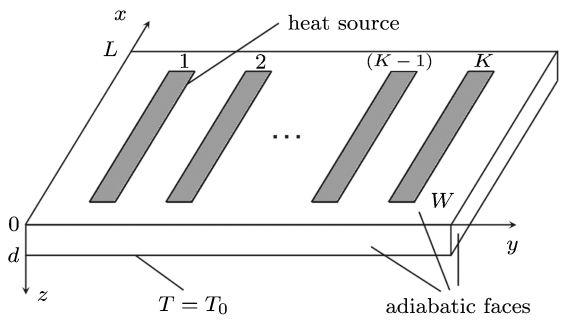


Fig. 1. Three-dimensional schematic structure of a K-finger power HBT.

*Project supported by the National Natural Science Foundation of China (Grant Nos. 61006059, 60776051, and 61006044), the Beijing Municipal Natural Science Foundation of China (Grant No. 4082007), the Beijing Municipal Education Committee of China (Grant Nos. KM200710005015 and KM200910005001), the Beijing Municipal Trans-century Talent Project of China (Grant No. 67002013200301), the Beijing Innovatory Talent Training Program of China (Grant No. 00200054RA001), and the Ph. D. Start Science Foundation of Beijing University of Technology of China (Grant No. X0002013201102).

†Corresponding author. E-mail: dyjin@bjut.edu.cn

© 2011 Chinese Physical Society and IOP Publishing Ltd

2. Thermal model

To account for thermal effects, a thermal network of the multi-finger HBT with a ground-referenced thermal voltage is shown in Fig. 2. In a multi-finger HBT, one can assign a constant temperature to each emitter finger (for example its average temperature). Therefore, the self-heating effect in thermal network can be represented as a parallel combination of R_{ii} and thermal current source (I_i) (which represents dissipation power (P_i) within the i-th emitter finger) and the self-heating temperature rise of the i-th finger is denoted as T_{Si} ($T_{Si} = R_{ii} \times P_i = R_{ii} \times I_i \times V_{\rm CE}$). Furthermore, the thermal coupling effect is represented as voltage sources summed in series with the thermal coupling temperature rise

$$T_{Ci} = \frac{R_{i1}}{R_{11}} T_{S1} + \cdots + \frac{R_{i(i-1)}}{R_{(i-1)(i-1)}} T_{S(i-1)} + \frac{R_{i(i+1)}}{R_{(i+1)(i+1)}} T_{S(i+1)} + \cdots + \frac{R_{iK}}{R_{KK}} T_{SK},$$

where T_{Ci} is the total thermal coupling temperature rise of the i-th finger, R_{im} ($m = 1, 2, \ldots, i-1, i+1, \ldots, K$) is the thermal coupling resistance which represents how finger m contributes to the temperature rise of finger i.

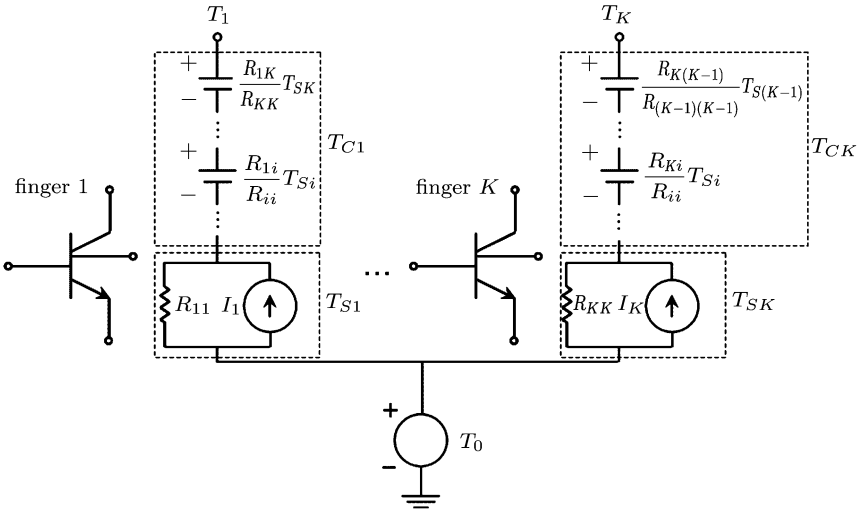


Fig. 2. Thermal network of a multi-finger HBT by taking into account self-heating and thermal coupling effects.

According to the thermal network of the multi-finger HBT, the thermal model can be defined by

$$T_i = T_{Si} + T_{Ci} + T_0 = \sum_{j=1}^{K} R_{ij} P_j + T_0, \qquad (1)$$

where T_i is the total temperature rise of finger i; P_j is the dissipated power delivered by finger j; $[R_{ij}]$ is the thermal resistance matrix, which fully describes the thermal properties of the device; R_{ij} is a symmetric matrix (where R_{ij}=R_{ji}) and it is determined by the distance between emitter fingers and the thermal conductivity of the substrate material. At the same time, $[R_{ij}]$ also has a marked effect on the temperature profile of the HBT and it can be calculated by solving the heat flow equation in a multi-finger device.

In a steady state, the heat flow equation is given by[8−10]

$$\nabla^2 T(x, y, z) = 0. \qquad (2)$$

Combined with the three-dimensional schematic structure of a multi-finger power HBT shown in Fig. 1, the appropriate boundary conditions are presented as follows:

$$T|_{z=d} = T_0, \qquad (3)$$

$$K_{\rm th} \left.\frac{\partial T}{\partial z}\right|_{z=0} = -p(x, y), \qquad (4)$$

$$\left.\frac{\partial T}{\partial x}\right|_{x=0,L} = 0, \qquad (5)$$

$$\left.\frac{\partial T}{\partial y}\right|_{y=0,W} = 0, \qquad (6)$$

where the bottom of the chip ($z = d$) is fixed at the ambient temperature T_0 (300 K in our study), the

heat source is assumed to be located on the top surface ($z = 0$) and $p(x, y)$ is a distribution function of input power density on top surfaces of the chip, which is zero except at the fingers where the device power is dissipated and $K_{\rm th}$ is the thermal conductivity of substrate materials.

With the aid of the separation of variables, the analytical solution of the heat flow equation (2) can be derived under the appropriate boundary conditions given by Eqs. (3)–(6). The expression of the temperature in the i-th emitter finger $T_i(x_i,\ y_i,\ 0)$ is given as[11,12]

$$\begin{aligned} T_i(x_i, y_i, 0) = {} & \frac{2w}{LW}\sum_{m=1}^{\infty}\left[\frac{1}{\lambda_m^2}\tanh(\lambda_m d)\cdot\sum_{i=1}^{K}\frac{p_i}{k_{\rm th}}\cdot F(m,i)\cdot\cos(\lambda_m x_i)\right] \\ & + \frac{2l}{LW}\sum_{n=1}^{\infty}\left[\frac{1}{\mu_n^2}\tanh(\mu_n d)\cdot\sum_{i=1}^{K}\frac{p_i}{k_{\rm th}}\cdot G(n,i)\cdot\cos(\mu_n y_i)\right] \\ & + \frac{4}{LW}\sum_{m=1}^{\infty}\sum_{n=1}^{\infty}\left[\frac{1}{\lambda_m\mu_n\gamma}\tanh(\gamma d)\cdot\sum_{i=1}^{K}\frac{p_i}{k_{\rm th}}\cdot F(m,i)\cdot G(n,i)\cdot\cos(\lambda_m x_i)\cdot\cos(\mu_n y_i)\right] \\ & + \frac{lwd}{LW}\sum_{i=1}^{K}\frac{p_i}{k_{\rm th}} + T_0, \end{aligned} \tag{7}$$

where

$$\lambda_m = m\pi/L,\quad \mu_n = n\pi/W,\quad \gamma^2 = \lambda_m^2 + \mu_n^2,$$
$$F(m,i) = \sin\lambda_m(x_i + l/2) - \sin\lambda_m(x_i - l/2),$$
$$G(n,i) = \sin\mu_n(y_i + w/2) - \sin\mu_n(y_i - w/2).$$

According to Eq. (7), the temperatures of the two (i and j) fingers T_i and T_j are first calculated under the same power level. By increasing the power of finger j with ΔP_j, a new temperature distribution is calculated. Therefore, thermal resistance matrix $[R_{ij}]$ including R_{ii} and $R_{ij(i\neq j)}$ is obtained by using the temperature rise of finger i, ΔT_i,

$$R_{ij} = \frac{\Delta T_i}{\Delta P_j}. \tag{8}$$

Taking a two-finger SiGe HBT for example, $R_{ij(i\neq j)}$ is calculated as a function of the finger spacing and shown in Fig. 3. The total emitter stripe area of the device is 400 μm^2, total collector current ($I_{\rm C}$) is 30 mA and voltage of collector–emitter ($V_{\rm CE}$) is 5 V. It is shown that $R_{ij(i\neq j)}$ decreases as finger spacing increases. Furthermore, for finger spacing larger than 10 μm, the trend of $R_{ij(i\neq j)}$ can be approximated by an exponential function and $R_{ij(i\neq j)}$ is lowered only by 14 K/W with finger spacing increasing from 30 μm to 50 μm, indicating that effective thermal coupling exists only when the two fingers are very close to each other. According to Eq. (1), the decrease of $R_{ij(i\neq j)}$ is helpful for lowering the emitter finger temperature, which sheds light on adopting non-uniform finger spacing structure to improve the thermal stability of multi-finger power HBTs.

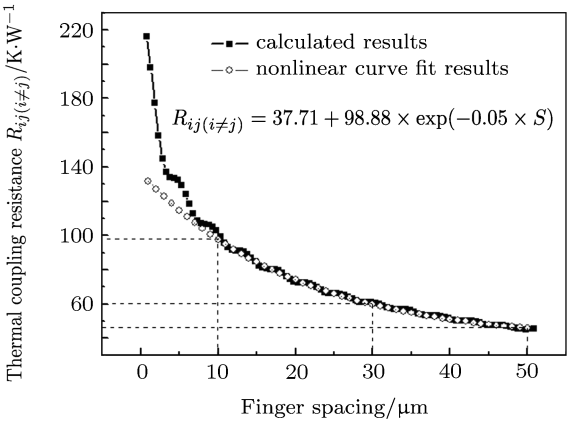


Fig. 3. Thermal coupling resistance ($R_{ij(i\neq j)}$) versus finger spacing in a two-finger HBT. The trend of $R_{ij(i\neq j)}$ can be approximated as an exponential function (shown in the figure) at large (> 10 μm) finger spacings.

3. Layout design

With the aid of the thermal model, $[R_{ij}]$ in a 10-finger HBT (HBT-1) with a total emitter stripe area of 400 μm^2 and a uniform finger spacing of 10.8 μm is calculated at $I_{\rm C}$ of 150 mA and $V_{\rm CE}$ of 5 V. At the same time, iterations are also used to calculate T_i and P_j of the device. First, it is assumed that there is an even collector current distribution across all fingers. Due to the thermal effects, the temperature of each emitter finger can be calculated with a temperature rise different from the others'. Because of

the positive temperature coefficient of I_{Ci} in Eq. (9), the collector current is redistributed and leads to a further non-uniform distribution of T_i.[13] The above steps are iterated until the final steady-state solutions are reached. The steady-state results of T_i, R_{ij} and P_j in HBT-1 are shown in Eq. (10). It can be seen that due to the thermal effects, neither the power level nor the finger temperature has a uniform distribution. In other words, both of them have higher values in the central fingers

$$I_{Ci} = I_{C0} \exp\left\{ \frac{q}{k_0 T_0} \left[V_{BE} \ -\phi(T(x_i, y_i, 0) - T_0) \right] \right\}, \tag{9}$$

where I_{C0} is the saturation current, k_0 is Boltzmann's constant, q is the charge of electron, $V_{\rm BE}$ and $V_{\rm CE}$ are the voltage of base–emitter and the collector–emitter, respectively.

In order to lower the finger temperature of central fingers and enhance the power level, the spacings between central fingers are increased to lower $R_{ij(i\neq j)}$, which can effectively suppress the heat flow from adjacent fingers. Meanwhile, the increase of finger spacing also widens the downward dissipation heat path and hence improves R_{ii}. At the same time, considering that the heat flow comes only from one direction of the outmost fingers, the outside finger spacings can be decreased moderately to keep the total finger spacing unchanged. A 10-finger HBT with non-uniform finger spacings of 7.8, 8.8, 10.8, 13.8, 14.8, 13.8, 10.8, 8.8, and 7.8 μm (HBT-2) is designed under the same power density of the uniform one. HBT-2 also has an identical vertical structure, total emitter stripes area and total spacing to those of the uniform one. The correlated T_i, $[R_{ij}]$ and P_i are shown in Eq. (11). The HBT-2 has a lower peak temperature of 328.15 K, which is lowered by 3.76 K and the non-uniformity of finger temperature is improved by 50.52%, when compared with that of HBT-1. The maximum power level difference of emitter finger is also improved by 51.33%. All of them are ascribed to the optimization of $[R_{ij}]$.

$$\begin{bmatrix} 319.38 \\ 324.7 \\ 328.44 \\ 330.7 \\ 331.91 \\ 331.91 \\ 330.7 \\ 328.44 \\ 324.7 \\ 319.38 \end{bmatrix} = \begin{bmatrix} 236.51 & 89.52 & 66.02 & 51.1 & 45.13 & 38.56 & 34.78 & 31.83 & 28.48 & 27.38 \\ 89.52 & 234.31 & 87.39 & 64.34 & 49.88 & 43.89 & 38 & 34.1 & 31.68 & 28.48 \\ 66.02 & 87.39 & 232.64 & 86.17 & 63.11 & 49.32 & 43.21 & 37.85 & 34.1 & 31.83 \\ 51.1 & 64.34 & 86.17 & 231.41 & 85.61 & 62.43 & 49.17 & 43.21 & 38 & 34.78 \\ 45.13 & 49.88 & 63.11 & 85.61 & 230.73 & 85.46 & 62.43 & 49.32 & 43.89 & 38.56 \\ 38.56 & 43.89 & 49.32 & 62.43 & 85.46 & 230.73 & 85.61 & 63.11 & 49.88 & 45.13 \\ 34.78 & 38 & 43.21 & 49.17 & 62.43 & 85.61 & 231.41 & 86.17 & 64.34 & 51.1 \\ 31.83 & 34.1 & 37.85 & 43.21 & 49.32 & 63.11 & 86.17 & 232.64 & 87.39 & 66.02 \\ 28.48 & 31.68 & 34.1 & 38 & 43.89 & 49.88 & 64.34 & 87.39 & 234.31 & 89.52 \\ 27.38 & 28.48 & 31.83 & 34.78 & 38.56 & 45.13 & 51.1 & 66.02 & 89.52 & 236.51 \end{bmatrix} \begin{bmatrix} 0.0627 \\ 0.07077 \\ 0.07705 \\ 0.08111 \\ 0.08337 \\ 0.08337 \\ 0.08111 \\ 0.07705 \\ 0.07077 \\ 0.0627 \end{bmatrix} + 273, \tag{10}$$

$$\begin{bmatrix} 321.95 \\ 326.49 \\ 328.15 \\ 327.37 \\ 326.61 \\ 326.61 \\ 327.37 \\ 328.15 \\ 326.49 \\ 321.95 \end{bmatrix} = \begin{bmatrix} 235.17 & 100.78 & 73.19 & 56.42 & 44.66 & 38.28 & 32.43 & 30.63 & 28.5 & 27.23 \\ 100.78 & 233.13 & 98.48 & 65.26 & 49.74 & 40.8 & 34.64 & 32.19 & 29.87 & 28.5 \\ 73.19 & 98.48 & 231.72 & 86.31 & 57.08 & 45.46 & 37.38 & 34.86 & 32.19 & 30.63 \\ 56.42 & 65.26 & 86.31 & 230.63 & 78.91 & 52.1 & 43.66 & 37.38 & 34.64 & 32.43 \\ 44.66 & 49.74 & 57.08 & 78.91 & 229.45 & 73.77 & 52.1 & 45.46 & 40.8 & 38.28 \\ 38.28 & 40.8 & 45.46 & 52.1 & 73.77 & 229.45 & 78.91 & 57.08 & 49.74 & 44.66 \\ 32.43 & 34.64 & 37.38 & 43.66 & 52.1 & 78.91 & 230.63 & 86.31 & 65.26 & 56.42 \\ 30.63 & 32.19 & 34.86 & 37.38 & 45.46 & 57.08 & 86.31 & 231.72 & 98.48 & 73.19 \\ 28.5 & 29.87 & 32.19 & 34.64 & 40.8 & 49.74 & 65.26 & 98.48 & 233.13 & 100.78 \\ 27.23 & 28.5 & 30.63 & 32.43 & 38.28 & 44.66 & 56.42 & 73.19 & 100.78 & 235.17 \end{bmatrix} \begin{bmatrix} 0.06829 \\ 0.07551 \\ 0.07835 \\ 0.07706 \\ 0.07579 \\ 0.07579 \\ 0.07706 \\ 0.07835 \\ 0.07551 \\ 0.06829 \end{bmatrix} + 273. \tag{11}$$

To further study the $[R_{ij}]$ distribution, the profiles of $[R_{ij}]$ in two types of devices are shown in Figs. 4(a) and 4(b), respectively. It is shown obviously that the diagonal R_{ii} is larger than $R_{ij(i\neq j)}$. At the same time, for HBT-1, the $R_{ij(i\neq j)}$ adjacent to diagonal R_{ii} is larger than the peripheral $R_{ij(i\neq j)}$,

which results in a higher temperature in the central fingers. However, for HBT-2, by adopting optimum non-uniform finger spacing structure, not only R_{ii} of each finger but also $R_{ij(i\neq j)}$ in the central fingers are decreased markedly, which can effectively improve the non-uniform distribution of T_i and P_j.

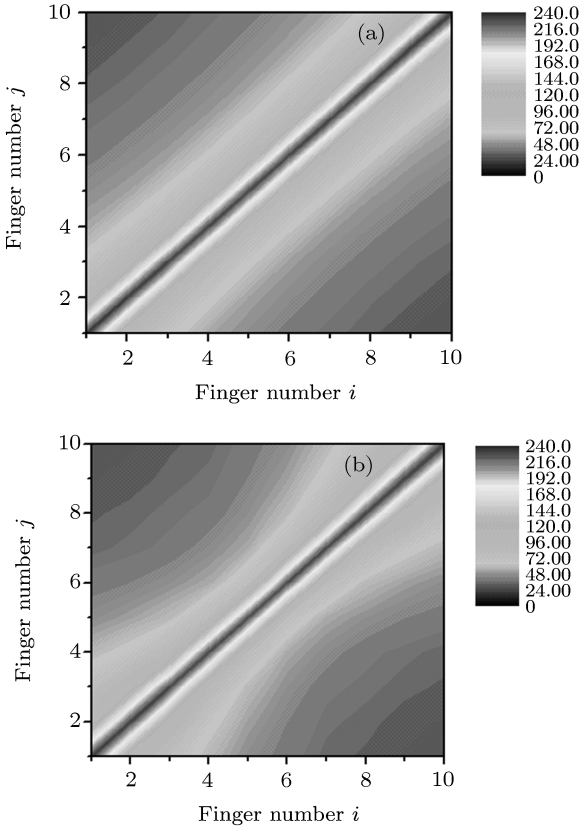


Fig. 4. Profiles of thermal resistance matrix $[R_{ij}]$ (K/W) of 10-finger HBTs with (a) uniform finger spacing (HBT-1) and (b) non-uniform finger (HBT-2) at $I_C = 150$ mA and $V_{\rm CE} = 5$ V.

As the voltage of collector–emitter $V_{\rm CE}$ increases to 7 V, the calculated correlated T_i, $[R_{ij}]$, and P_i in two devices are shown in expressions (12) and (13), respectively, where a lower self-heating thermal resistance and a more uniform $[R_{ij}]$ distribution are calculated in HBT-2 when compared with those of HBT-1. The comparisons of P_i values in two devices at different I_C values are presented in Fig. 5. It is shown that for both devices, the difference in power level between fingers is small at $V_{\rm CE} = 5$ V. As $V_{\rm CE}$ increases to 7 V, the differences in power level are obvious. The maximum power level difference for HBT-1 is approximately 75.4 mW, while it is only 27.8 mW for HBT-2 with an improvement of 63.13% in uniformity of power level distribution. Figure 6 shows the temperature profiles in two devices at different $V_{\rm CE}$ values. It is observed that for HBT-2, both the maximum values and the uniformities of T_i and P_i are significantly improved due to the improvement of $[R_{ij}]$. Specifically, the improvement of the peak temperature is increased from 5.3 K to 14.91 K, while the non-uniformity of the temperature profile is improved from 50.52% to 61.88% and more improvement in the non-uniformity of T_i is obtained in the central 6 fingers. It is evident that HBT-2 has a lower peak temperature and more uniform temperature profile which provides higher power-handling capability.

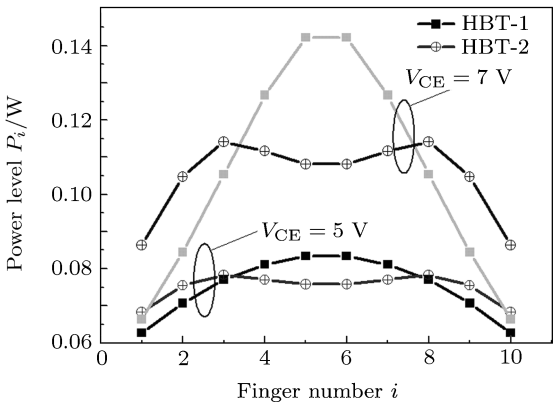


Fig. 5. Power levels of fingers at $V_{\rm CE} = 5$ V and $V_{\rm CE} = 7$ V for the HBT with uniform finger spacing (HBT-1) (■) and HBT with non-uniform finger spacing (HBT-2) (⊕).

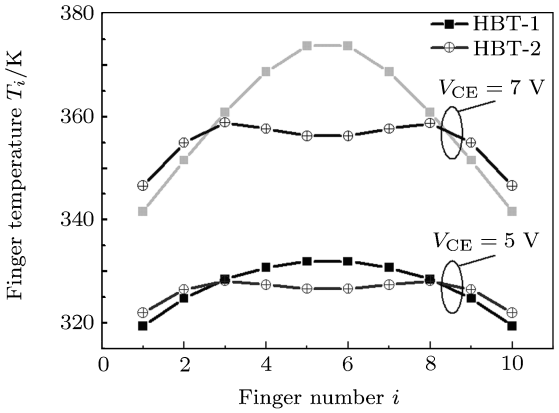


Fig. 6. Temperatures of fingers at $V_{\rm CE} = 5$ V and $V_{\rm CE} = 7$ V for the HBT with uniform finger spacing (HBT-1) (■) and HBT with non-uniform finger spacing (HBT-2) (⊕).

$$\begin{bmatrix} 341.58 \\ 351.55 \\ 360.89 \\ 368.74 \\ 373.79 \\ 373.79 \\ 368.74 \\ 360.89 \\ 351.55 \\ 341.58 \end{bmatrix} = \begin{bmatrix} 267.79 & 101.36 & 74.74 & 57.86 & 51.09 & 43.66 & 39.38 & 36.04 & 32.25 & 31.01 \\ 101.36 & 265.3 & 98.95 & 72.86 & 56.48 & 49.69 & 43.03 & 38.61 & 35.87 & 32.25 \\ 74.74 & 98.95 & 263.42 & 97.56 & 71.46 & 55.84 & 48.93 & 42.86 & 38.61 & 36.04 \\ 57.86 & 72.86 & 97.56 & 262.02 & 96.93 & 70.69 & 55.67 & 48.93 & 43.03 & 39.38 \\ 51.09 & 56.48 & 71.46 & 96.93 & 261.24 & 96.76 & 70.69 & 55.84 & 49.69 & 43.66 \\ 43.66 & 49.69 & 55.84 & 70.69 & 96.76 & 261.24 & 96.93 & 71.46 & 56.48 & 51.09 \\ 39.38 & 43.03 & 48.93 & 55.67 & 70.69 & 96.93 & 262.02 & 97.56 & 72.86 & 57.86 \\ 36.04 & 38.61 & 42.86 & 48.93 & 55.84 & 71.46 & 97.56 & 263.42 & 98.95 & 74.74 \\ 32.25 & 35.87 & 38.61 & 43.03 & 49.69 & 56.48 & 72.86 & 98.95 & 265.3 & 101.36 \\ 31.01 & 32.25 & 36.04 & 39.38 & 43.66 & 51.09 & 57.86 & 74.74 & 101.36 & 267.79 \end{bmatrix} \begin{bmatrix} 0.06642 \\ 0.08439 \\ 0.10536 \\ 0.12666 \\ 0.14216 \\ 0.14216 \\ 0.12666 \\ 0.10536 \\ 0.08439 \\ 0.06642 \end{bmatrix} + 273, \quad (12)$$

$$\begin{bmatrix} 346.6 \\ 354.99 \\ 358.88 \\ 357.7 \\ 356.29 \\ 356.29 \\ 357.7 \\ 358.74 \\ 354.99 \\ 346.6 \end{bmatrix} = \begin{bmatrix} 258.57 & 110.8 & 80.47 & 62.03 & 49.1 & 42.09 & 35.66 & 33.68 & 31.34 & 29.94 \\ 110.8 & 256.32 & 108.28 & 71.75 & 54.69 & 44.86 & 38.08 & 35.4 & 32.85 & 31.34 \\ 80.47 & 108.28 & 254.78 & 94.89 & 62.75 & 51.3 & 41.1 & 38.33 & 35.4 & 33.68 \\ 62.03 & 71.75 & 94.89 & 253.58 & 86.76 & 57.29 & 48 & 41.1 & 38.08 & 35.66 \\ 49.1 & 54.69 & 62.75 & 86.76 & 252.27 & 81.11 & 57.29 & 49.98 & 44.86 & 42.09 \\ 42.09 & 44.86 & 49.98 & 57.29 & 81.11 & 252.27 & 86.76 & 62.75 & 54.69 & 49.1 \\ 35.66 & 38.08 & 41.1 & 48 & 57.29 & 86.76 & 253.58 & 94.89 & 71.75 & 62.03 \\ 33.68 & 35.4 & 38.33 & 41.1 & 49.98 & 62.75 & 94.89 & 254.78 & 108.28 & 80.47 \\ 31.34 & 32.85 & 35.4 & 38.08 & 44.86 & 54.69 & 71.75 & 108.28 & 256.32 & 110.8 \\ 29.94 & 31.34 & 33.68 & 35.66 & 42.09 & 49.1 & 62.03 & 80.47 & 110.8 & 258.57 \end{bmatrix} \begin{bmatrix} 0.08635 \\ 0.10477 \\ 0.11415 \\ 0.11163 \\ 0.10811 \\ 0.10811 \\ 0.11163 \\ 0.11415 \\ 0.10477 \\ 0.08635 \end{bmatrix} + 273. \quad (13)$$

4. Conclusions

To represent the thermal effects, the $[R_{ij}]$ of multi-finger power HBTs including R_{ii} and $R_{ij(i\neq j)}$ is presented in the paper. The $R_{ij(i\neq j)}$ is calculated with the aid of heat flow equation and it is shown that $R_{ij(i\neq j)}$ decreases as finger spacing increases, which can be approximated by an exponential function. It also sheds light on the improvement of the thermal stability of the device with a non-uniform finger spacing structure. Taking a 10-finger power HBT for example, the non-uniform finger spacing structure is designed. By increasing the spacing between central fingers, both R_{ii} and $R_{ij(i\neq j)}$ are decreased, which effectively lowers the peak temperature and improves the non-uniformity of the temperature profile when compared with those of the uniform finger spacing case. For the optimized device with non-uniform finger spacing, as $V_{\rm CE}$ increases from 5 V to 7 V, the improvement of the peak temperature is increased from 5.3 K to 14.91 K, while the non-uniformity of the temperature profile is improved from 50.52% to 61.88%, indicating that the optimized device can effectively operate at higher power level and provides higher power-handling capability. Our research provides a useful guide for designing thermal stable power HBTs.

References

[1] Avenier G, Diop M, Chevalier P, Troillard G, Loubet N, Bouvier J, Depoyan L, Derrier N, Buczko M, Leyris C, Boret S, Montusclat S, Margain A, Pruvost S, Nicolson S T, Yau K H K, Revil N, Gloria D, Dutartre D, Voinigescu S P and Chantre A 2009 *IEEE J. Solid-State Circuits* **44** 2312

[2] Kim H S, Kim K Y, Kim W Y, Noh Y S, Yom I B, Oh I Y and Park C S 2009 *Electron. Lett.* **45** 1036

[3] Li X J, Geng H B, Lan M J, Yang D Z, He S Y and Liu C M 2010 *Chin. Phys.* B **19** 066103

[4] Zhang Y R, Zhang B, Li Z H, Lai C J and Li Z J 2009 *Chin. Phys.* B **18** 763

[5] Jin D Y, Zhang W R, Shen P, Xie H Y, Wang Y and Zhang W 2008 *Solid-State Electron.* **52** 937

[6] Zhou S L, Huang H, Huang Y Q and Ren X M 2007 *Acta Phys. Sin.* **56** 2890 (in Chinese)

[7] Hu H Y, Zhang H M, Lu Y, Dai X Y, Hou H, Ou J F, Wamg W and Wang X Y 2006 *Acta Phys. Sin.* **55** 403 (in Chinese)

[8] Cheng R J and Ge H X 2010 *Chin. Phys.* B **19** 090201

[9] Kou J L, Lu H J, Wu F M and Xu Y S 2009 *Chin. Phys.* B **18** 1553

[10] Liu X M, Li B C and Huang Q P 2010 *Chin. Phys.* B **19** 097201

[11] Gao G B, Wang M Z, Gui X and Morkoc H 1989 *IEEE Trans. Electron. Dev.* **36** 854

[12] Jin D Y, Zhang W R, Xie H Y, Chen L, Shen P and Hu N 2009 *Microelectronics Reliability* **49** 382

[13] Jin D Y, Zhang W R, Xie H Y, Shen P and Wang Y 2008 *Journal of Beijing University of Technology* **34** 141 (in Chinese)